

# The near-Earth asteroids population from two decades of observations

Pasquale Tricarico

*Planetary Science Institute, 1700 East Fort Lowell, Suite 106, Tucson, AZ 85719, USA*

tricaric@psi.edu

## ABSTRACT

Determining the near-Earth asteroids (NEAs) population is the focus of intense research, with the most recent models converging to a population of approximately 1,000 km-sized NEAs and up to approximately  $10^8$  NEAs with absolute magnitude  $H < 28$ . Here we show that the NEAs population is significantly smaller than previous estimates, with  $900 \pm 10$  NEAs larger than 1 km, approximately 10% lower than most recent estimates. Additionally, we estimate the population of small NEAs at  $430,000 \pm 30,000$  for  $H < 28$ , a decrease by two orders of magnitude. These results are enabled by an analysis of the combined observations of nine of the leading asteroid surveys over the past two decades. This reduced population tracks very accurately the orbital distribution of recently discovered large NEAs, and produces an estimated Earth impact rate for small NEAs in good agreement with the bolide data. Data hint at a possible decrease of the average albedo in small NEAs that would reconcile the small difference between predicted bolide rates and observations, as well as explain the dip in the size-frequency distribution at a size of approximately 100 m. These results bring to focus the current status of the NEAs search activities, as we are in the endgame stage for larger NEAs, and knowing the statistical orbital distribution of the remaining asteroids will facilitate the development of optimal search strategies for current and future surveys.

## 1. Introduction

With an observed population exceeding 13,000 bodies, up from a few hundred only two decades ago, NEAs represent a threat of impact with Earth, as well as targets for robotic and human exploration, and a potential for in-space resource utilization. In order to estimate the NEAs population, the techniques typically adopted include the characterization of the detection efficiency of a reference survey and subsequent simulated detection of a synthetic population (Rabinowitz et al. 2000; Stuart and Binzel 2004; Mainzer et al. 2011), or the statistical tracking of NEAs from their

source regions in the main belt to the inner solar system and subsequent comparison to the detections by a reference survey (Bottke et al. 2002; Morbidelli et al. 2002), or the combination of these two approaches (Granvik et al. 2016). The re-detection of NEAs has also been used to estimate the level of completeness in the search of NEAs (Harris and D’Abramo 2015). The first approach is typically adopted by single-survey studies which have access to all the observing data and meta-data and can accurately assess the detection efficiency, and this has limited in the past the adoption of this approach on a multi-survey scale. The other approaches require the introduction of ad-hoc weights on the contributions of source regions, or bootstrapping procedures in order to generate NEAs population close to the observed one, and these *tuning* procedures are undesirable as they make it difficult to appreciate how much of the final agreement with observations is due to the predictive power of the model and how much is due instead to the model’s flexibility.

An opportunity to produce an improved NEAs population model comes from the development of a survey characterization technique which relies only on publicly available observational data. This technique was recently used to analyze the large volume of observational data (10,033 nights over two decades) from nine of the most active asteroid surveys (Tricarico 2016), to determine their nightly detection efficiency as a function of asteroid apparent magnitude and apparent velocity. We present the NEAs population estimate methods in §2, including an assessment of the trailing loss, the role of commensurability with the Earth’s orbit period, and the computation of the Earth impact rate. Then in §3 we present the main results: the NEAs population as a function of absolute magnitude, the orbital distribution, and the comparison to bolide data. In §4 we discuss the origin of the differences of our estimated NEAs population compared to previous results, and look in detail at the the possible decrease of geometric albedo in small NEAs. Conclusions are briefly drawn in §5.

## 2. Methods

The baseline analysis of the observational data (Tricarico 2016) included only observations at apparent velocities up to 100 arcsec/hour, while NEAs can move at several deg/day, so we need to extend this analysis here and include the possible effect of trailing losses. Trailing losses can be important for asteroids with large apparent velocities, and this becomes even more important when including very small asteroids which are only visible when close to the Earth and thus move fast in the sky. In practice, approximately 90% of all NEAs observations are at apparent velocities below 3 deg/day, and approximately 99% below 10 deg/day. The trailing loss effects can be estimated directly from data, see Fig. 1, and the best linear fit is:

$$\eta_{\text{trail}} = (1.019 \pm 0.032) - (0.016 \pm 0.008)U \quad (1)$$

where the apparent velocity  $U$  is expressed in deg/day, the uncertainties quoted are  $1\sigma$ , and the reduced chi-squared is  $\tilde{\chi}^2 = 0.35$ . In the limit of low apparent velocity we have  $\eta_{\text{trail}} \simeq 1$  indicating that the detection efficiency fits from the baseline analysis apply to slow NEAs as well. When applying this correction, it is capped to be  $0 \leq \eta_{\text{trail}} \leq 1$  similarly to the other modeled efficiency curves (Tricarico 2016).

The progress in searching for NEAs is tracked by generating a large number ( $\sim 10^7$ ) of synthetic NEAs, and then numerically propagating their orbits over the two decades period considered, while checking against the sky coverage and detection efficiency of the surveys (Tricarico 2016). For every night  $j$  in which the synthetic asteroid appears in the field of view of a survey, a detection efficiency  $\eta_j(V, U)$  can be associated to it, as a function of apparent magnitude  $V$  and apparent velocity  $U$ . We can then calculate the completeness  $C$  of the search of the synthetic NEA as

$$C = 1 - \prod_j (1 - \eta_j). \quad (2)$$

This relation can be derived considering that the probability of *not* being detected the night  $j$  is  $1 - \eta_j$ , the product over  $j$  indicates the probability of not being detected any of the  $j$  nights, so that  $C$  is the probability of being detected at least on one night. Both  $\eta_j$  and  $C$  take values between 0 and 1. The completeness  $C$  is larger than or equal to the largest  $\eta_j$  and never decreases as nights accumulate. As we show in Figure 2, some orbits can be significantly more difficult to search due to close commensurability with the Earth’s orbit period, which causes the persistency of unfavorable observing geometries. In general, high inclination orbits are more difficult to search, as well as high eccentricity orbits for semi-major axis larger 1 AU, while low eccentricity orbits are more difficult to search for semi-major axis up to 1 AU.

The synthetic NEAs and corresponding completeness values are binned in the orbital elements space as follows: semi-major axis from 0.5 AU to 5.0 AU in increments of 0.05 AU; eccentricity from 0 to 1 in increments of 0.05; inclination from  $0^\circ$  to  $90.0^\circ$  in increments of  $5^\circ$ ; longitude of the ascending node, argument of perihelion, and mean anomaly from  $0^\circ$  to  $360^\circ$  in increments of  $30^\circ$ . By definition, all NEAs have orbits with a perihelion distance smaller than 1.3 AU. The absolute magnitude  $H$  is sampled from 8 to 28 in increments of 1 magnitude. The binning choice captures the typical scale over which the completeness  $C$  changes, as we can see from Figure 2. The completeness  $C_i$  associated to each bin  $i$  is then the average value, and the corresponding uncertainty  $\sigma_{C_i}$  is the statistical average error.

The bin population  $n_i$  is estimated using the negative binomial statistics, with  $k_i$  the number of known NEAs observed in the same bin, and  $C_i$  the completeness value of the bin. The probability for each possible value of  $n_i \geq k_i$  is

$$P(n_i, k_i, C_i) = \frac{(n_i - 1)!}{(k_i - 1)!(n_i - k_i)!} C_i^{k_i} (1 - C_i)^{n_i - k_i} \quad (3)$$

with mean  $n_i = k_i/C_i$  and standard deviation  $\sigma_{n_i}^2 = k_i(1 - C_i)/C_i^2$ . When used to estimate the bin population, the uncertainty  $\sigma_{C_i}$  of the completeness is propagated to obtain  $\sigma_{n_i}^2 = k_i(1 - C_i)/C_i^2 + k_i^2\sigma_{C_i}^2/C_i^4$ , and when sampling synthetic NEAs we require that the contribution of the  $\sigma_{C_i}$  term to  $\sigma_{n_i}$  is smaller than  $0.01\sigma_{n_i}$ .

The impact rate of synthetic NEAs with Earth is computed using standard techniques (Kessler 1981) accurately validated on known test cases (Bottke and Greenberg 1993), and includes an effective Earth cross section  $\sigma_E = \pi R_E^2(1 + v_{\text{esc}}^2/v_\infty^2)$  enhanced by gravitational focusing, with  $R_E$  Earth radius,  $v_{\text{esc}}$  Earth escape velocity, and  $v_\infty = v_{\text{ast}} - v_E$  the orbital intersection velocity of the asteroid relative to Earth ignoring the Earth’s gravitational pull. The distribution of  $v_\infty$  is typically wide and irregular (Bottke et al. 1994), and we track both the mean and standard deviation values when estimating the range of possible values for synthetic NEAs within a bin, which is sufficient in the central limit for a sufficiently large number of samples. The Earth impact velocity is then  $v_{\text{imp}}^2 = v_{\text{esc}}^2 + v_\infty^2$ .

### 3. Results

The resulting population debiasing procedure is free of tunable parameters, and produces a cumulative NEAs population model as a function of absolute magnitude, see Table 1 and Figure 3 where it is displayed along with previous results by other studies. We estimate  $900 \pm 10$  NEAs with absolute magnitude  $H < 17.75$ , roughly corresponding to asteroids larger than 1 km at a nominal average geometric albedo  $p_V = 0.14$  (Stuart and Binzel 2004). This a significant reduction (approximately 10% lower) compared to recent results (Mainzer et al. 2011; Harris and D’Abramo 2015; Granvik et al. 2016) which converged to approximately 1,000 large NEAs, and brings the current search completion level to over 97% for large NEAs. Earlier works (Rabinowitz et al. 2000; Morbidelli et al. 2002) had estimates compatible with ours, although with larger uncertainties. We also estimate  $20,000 \pm 1000$  NEAs with absolute magnitude  $H < 22.75$ , roughly corresponding to asteroids larger than 100 m, in good agreement with NEOWISE (Mainzer et al. 2011) but significantly lower than more recent results (Harris and D’Abramo 2015; Granvik et al. 2016). The data available allow to estimate the small NEAs population for  $H < 28$  at  $430,000 \pm 30,000$ , approximately two orders of magnitude lower than Harris and D’Abramo (2015).

Our reduced NEAs population model can be tested against the current discoveries of large NEAs. In Figure 4 we show the orbital distribution of the  $H < 17.75$  population. As we can see, the estimated population, which used input observations up to August 2014, predicts very closely the current observed population including the NEAs discovered during the following 18 months up to February 2016. Note also from Figure 4a how the bins where yet undiscovered NEAs are expected correlates with commensurabilities with the Earth’s orbital period. Additionally, most of

the expected remaining large NEAs have an eccentricity larger than 0.55. Since NEAs with orbit periods commensurate to the Earth’s one are more difficult to detect, targeted search strategies may be necessary for faster progress, especially for the remaining large NEAs. Space-based surveys could alleviate the problem but would need to be in heliocentric orbits with periods significantly shorter or longer than one year, and this would cause the spacecraft to drift away from Earth over time, influencing negatively the communications.

We expect the orbital distribution to depend on  $H$ . In semi-major axis (see Figure 6), the distribution at increasing  $H$  tends to become more flat between 1.1 AU and 2.5 AU, and rapidly decay outside this range. In eccentricity (see Figure 7), at increasing  $H$  we tend to lose high-eccentricity NEAs. The effective maximum inclination of NEAs tends to reduce with increasing  $H$ , with most NEAs below  $45^\circ$  for  $H < 22$ , below  $35^\circ$  for  $H < 24$ , and below  $15^\circ$  for  $H < 28$ , see Figure 8.

This NEAs population can also be tested against the observed rate of bolides (Brown et al. 2013), and in Figure 5 we compare their impact rate versus impact energy with ours. The bolide observations seem to overlap with the modeled NEAs impact rates in the small energy range around  $10^2$  kt, and then set to a slightly higher average power law at lower impact energies. The uncertainty in bolide data represents only counting statistics, and there could be some systematic uncertainties in some of the model assumptions (i.e. from mean optical to total energy conversion) capable of producing a shift of the order of a factor two (P. Brown, *priv. comm.*).

#### 4. Discussion

There are several factors which contribute to an overall reduction of the estimated NEAs population compared to previous studies. The trailing loss estimated from data in Eq. (1) decays very slowly at high apparent velocities, meaning that surveys are losing fewer fast NEAs than previously thought, and this reduces the NEAs population estimate especially for small NEAs. But the main issue is that of the completeness estimation, which is used to project the known population to the total estimated population, and lower completeness levels in previous studies (sometimes lower by orders of magnitude for small NEAs) cause an amplified population estimate. As we mentioned in Tricarico (2016), very slow NEAs cause a decrease in detection efficiency, and if this effect is not modeled carefully, it may be confused for an effectively lower overall detection efficiency for a single night, and then propagate into lower completeness values.

Earlier works generated bolide rates estimates from NEAs in good agreement with observations (Brown et al. 2013; Harris and D’Abramo 2015), qualitatively similar to what we obtain here, even if the population size differs by orders of magnitude. One explanation for this apparent para-

dox is in the calculation of the impact probabilities. Earlier studies used a single average value for the intrinsic impact probability with Earth of  $2 \times 10^{-9} \text{ year}^{-1}$ , while we have calculated it explicitly for every NEAs population bin, obtaining values approximately between  $10^{-3}$  and  $10^{-10} \text{ year}^{-1}$ , indicating that a detailed assessment of the impact probability is necessary. The impact velocities vary between the Earth escape velocity of  $11.2 \text{ km s}^{-1}$  up to approximately  $45 \text{ km s}^{-1}$ , so in order to obtain accurate estimates of the impact energy the impact velocity should be estimated for each population bin as well.

The small difference between the observed bolides rate and the modeled rate deduced from the NEAs population leaves open the intriguing possibility of an average albedo decrease in small NEAs, down to a value  $p_V \simeq 0.05$  (see Figure 9) which would cause the modeled Earth impact rate to match the observed bolide observations. For illustrative purposes we have calculated the effect that this albedo decrease would have on the size-frequency distribution, see Figure 10, where it compensates for the dip around 100 m, possibly slightly over-compensating for it. Additionally, the limited NEOWISE albedo observations Mainzer et al. (2011) of NEAs with size below 200 m show a decrease of the maximum albedo, from  $p_V$  up to 0.5 at 200 m to  $p_V$  up to 0.3 at 100 m size, supporting a possible decrease of average albedo at this size range. If small NEAs are on average darker than previously thought, this will significantly shorten the warning times (Chesley and Spahr 2004) for early warning systems using optical telescopes for impacts by NEAs of equivalent size.

A detailed understanding of the NEAs population independent of the source regions in the main belt offers novel opportunities to model the main asteroid belt population down to a size range which is still largely unconstrained by observations.

## 5. Conclusions

We have used the combined observations of asteroid surveys over the past two decades to model the NEAs population, obtaining significantly reduced population estimates compared to previous studies. The number of NEAs larger than 1 km yet to be discovered is now down to a few tens only, and this causes slow progress which may be accelerated by developing targeted search strategies. The high-resolution NEAs population obtained here is capable of accurately predict the statistical orbit distribution of recent discoveries, thus demonstrating the potential to develop search strategies targeted not only at the remaining large NEAs, but also at smaller NEAs with potential Earth impact probabilities significantly higher than average. The possible darkening of smaller NEAs raises the possibility of significantly shorter warning times for potential impacts by asteroid of equivalent size.

This research is supported by the NASA Near Earth Object Observations (NEOO) Program grant NNX13AQ43G, and by the NASA Applied Information System Research (AISR) Program grant NNX08AD18G. We thank Peter Brown for correspondence on bolide observations. Early versions of this research made use of the BOINC-based (Anderson 2004) orbit@home distributed computing network, and the participants who donated computing time on their personal computers are acknowledged.

## REFERENCES

- Anderson, D. P. 2004. BOINC: a system for public-resource computing and storage. Proceedings of the Fifth IEEE/ACM International Workshop on Grid Computing (GRID04), 4-10.
- Bottke, W. F., Greenberg, R. 1993. Asteroidal collision probabilities. *Geophysical Research Letters* 20, 879-881.
- Bottke, W. F., Nolan, M. C., Greenberg, R., Kolvoord, R. A. 1994. Velocity distributions among colliding asteroids. *Icarus* 107, 255-268.
- Bottke, W. F., Morbidelli, A., Jedicke, R., Petit, J.-M., Levison, H. F., Michel, P., Metcalfe, T. S. 2002. Debaised Orbital and Absolute Magnitude Distribution of the Near-Earth Objects. *Icarus* 156, 399-433.
- Brown, P. G., and 32 colleagues 2013. A 500-kiloton airburst over Chelyabinsk and an enhanced hazard from small impactors. *Nature* 503, 238-241.
- Chesley, S. R., Spahr, T. B. 2004. Earth impactors: orbital characteristics and warning times. *Mitigation of Hazardous Comets and Asteroids* 22.
- Granvik, M., Morbidelli, A., Jedicke, R., Bolin, B., Bottke, W. F., Beshore, E., Vokrouhlický, D., Delbò, M., Michel, P. 2016. Super-catastrophic disruption of asteroids at small perihelion distances. *Nature* 530, 303-306.
- Harris, A. W., D’Abramo, G. 2015. The population of near-Earth asteroids. *Icarus* 257, 302-312.
- Kessler, D. J. 1981. Derivation of the collision probability between orbiting objects The lifetimes of Jupiter’s outer moons. *Icarus* 48, 39-48.
- Mainzer, A., and 36 colleagues 2011. NEOWISE Observations of Near-Earth Objects: Preliminary Results. *The Astrophysical Journal* 743, 156.
- Morbidelli, A., Jedicke, R., Bottke, W. F., Michel, P., Tedesco, E. F. 2002. From Magnitudes to Diameters: The Albedo Distribution of Near Earth Objects and the Earth Collision Hazard. *Icarus* 158, 329-342.
- Rabinowitz, D., Helin, E., Lawrence, K., Pravdo, S. 2000. A reduced estimate of the number of kilometre-sized near-Earth asteroids. *Nature* 403, 165-166.
- Stuart, J. S., Binzel, R. P. 2004. Bias-corrected population, size distribution, and impact hazard for the near-Earth objects. *Icarus* 170, 295-311.
- Tricarico, P. 2016. Detection Efficiency of Asteroid Surveys. *The Astronomical Journal* 151, 80.



Table 1. Cumulative NEAs Population

$H$	observed	known	estimated population		
10	1	1	1.0	±	0.0
11	1	1	1.0	±	0.0
12	2	2	2.0	±	0.0
13	5	5	5.0	±	0.0
14	15	15	15.0	±	0.0
15	54	54	54.0	±	0.1
16	167	167	168.7	±	1.5
17	442	447	454.3	±	4.3
18	987	1022	1057.8	±	11.6
19	2032	2174	2395.8	±	29.8
20	3363	3737	4800.0	±	93.1
21	4675	5397	8773.5	±	276.6
22	5776	6848	13817.1	±	373.3
23	6709	8130	23042.2	±	1016.7
24	7674	9506	43076.2	±	2230.3
25	8720	10968	88322.8	±	5135.9
26	9525	12141	175620.2	±	13211.8
27	10106	13027	302818.8	±	17880.2
28	10386	13463	425869.3	±	24761.5

Note. — Columns: upper bound absolute magnitude  $H$ , cumulative number of NEAs observed during the baseline survey period up to August 2014 (Tricarico 2016), cumulative number of known NEAs as of February 2016, and full population as estimated in this manuscript.

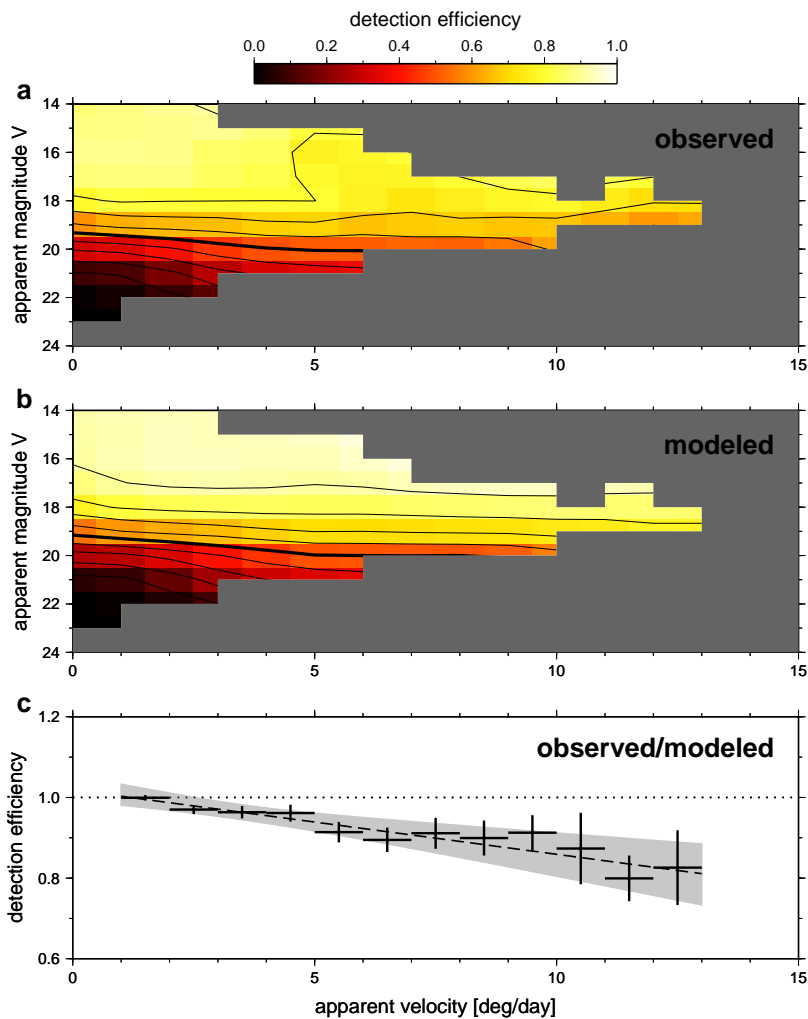


Fig. 1.— (a) observed and (b) modeled detection efficiency for NEAs. Data are binned 1 deg/day by 1 magnitude, and only bins with a relative uncertainty smaller than 0.1 are included, while bins with larger uncertainty or with no data are grey. Level curves are at intervals of 0.1, with the bold level curve marking the 0.5 value. The modeled detection efficiency uses the nightly fits as described in Tricarico (2016). (c) correction factor to the nightly detection efficiency due to trailing loss, obtained as the bin-by-bin ratio of observed/modeled, and then weight-averaged over the apparent magnitude. The dashed line marks the linear fit of  $\eta_{\text{trail}} = 1.019 - 0.016U$  with  $U$  in deg/day, and the grey region represents the  $1\sigma$  uncertainty.

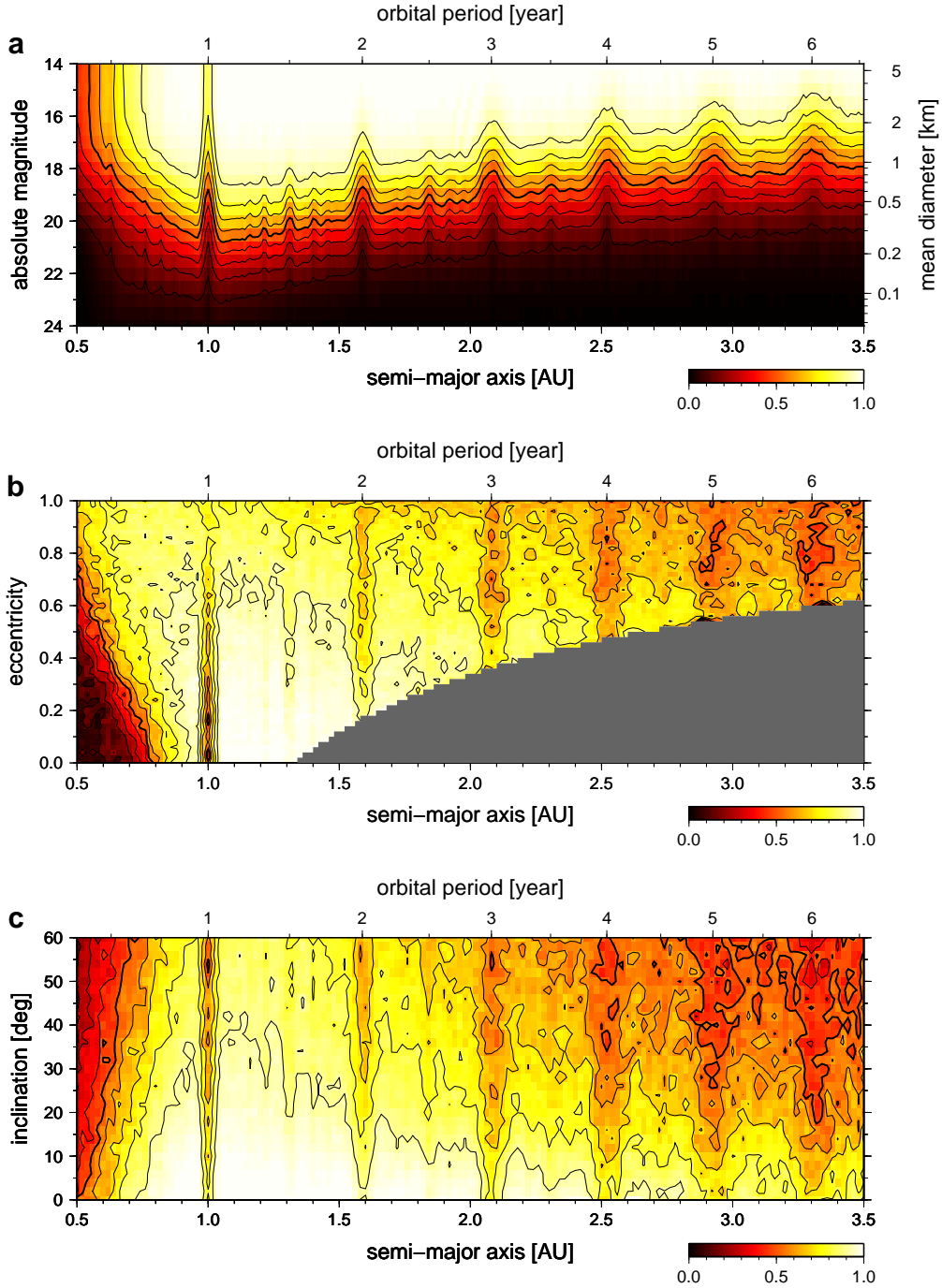


Fig. 2.— Completeness in the search of NEAs (color scale) projected on: (a) absolute magnitude vs. semi-major axis, averaged over orbits with eccentricity between 0 and 1, and inclination between  $0^\circ$  and  $60^\circ$ , with a mean diameter assuming a nominal geometric albedo  $p_V = 0.14$ ; (b) eccentricity vs. semi-major axis for NEAs with absolute magnitude  $H < 20$ , averaged over inclination between  $0^\circ$  and  $60^\circ$ ; (c) inclination vs. semi-major axis for NEAs with absolute magnitude  $H < 20$ , averaged over orbits with eccentricity between 0 and 1. Note the effect of commensurability in orbit period of NEA and Earth, not just the integer multiples but also fractional ones.

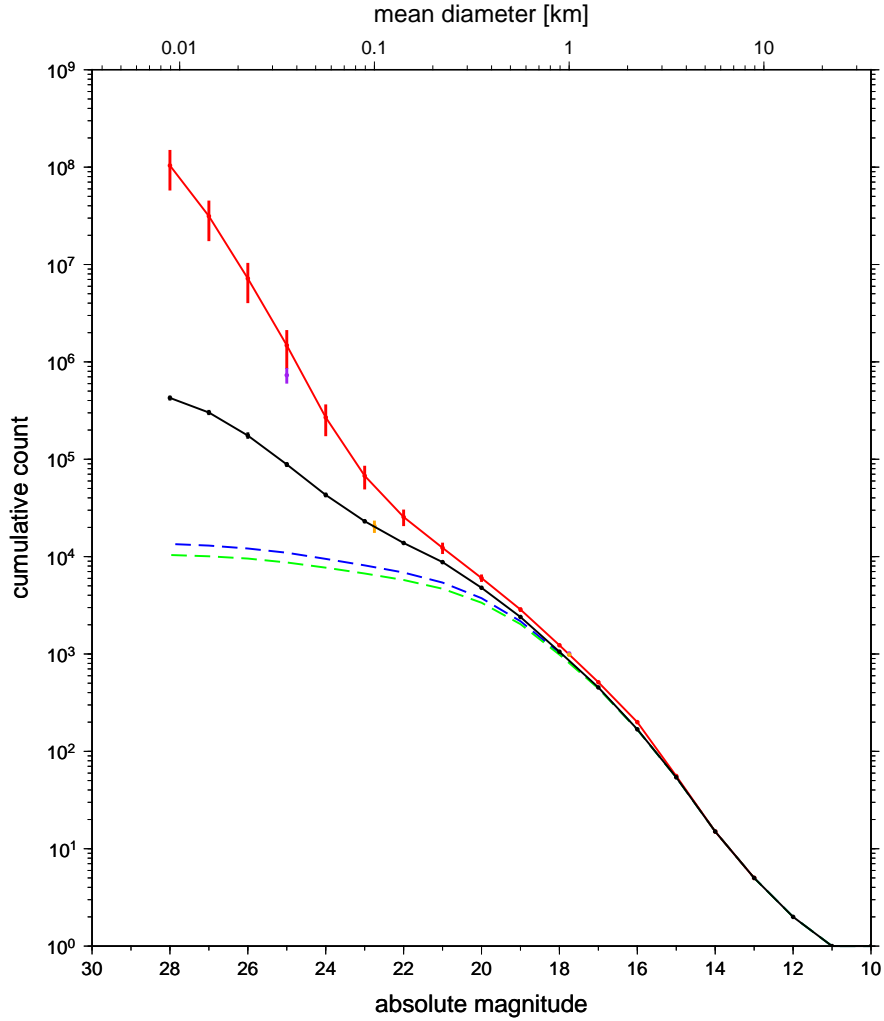


Fig. 3.— Cumulative NEAs population as a function of absolute magnitude. The black data are our estimated population, where the error bars are present but small, see Table 1. The orange data are from Mainzer et al. (2011), the red from Harris and D’Abramo (2015), the purple from Granvik et al. (2016). The dashed green data are the observed NEAs population used as input (observed during the baseline period Tricarico (2016) up to August 2014), while the blue data are the full known NEAs population as of February 2016. The mean diameter is for reference and assumes a nominal geometric albedo  $p_V = 0.14$ .

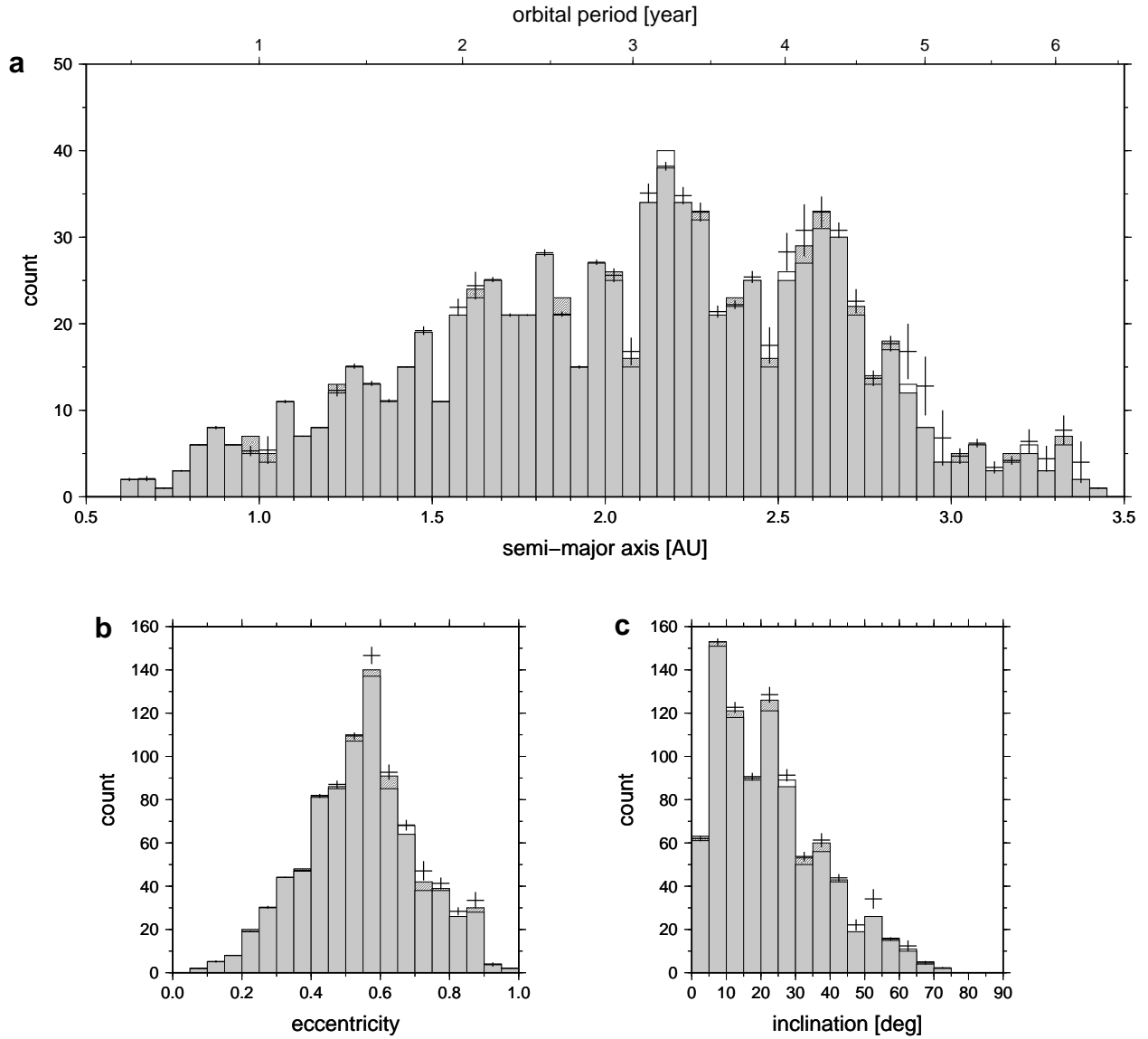


Fig. 4.— Distribution of NEAs with  $H < 17.75$  versus (a) semi-major axis, (b) eccentricity, (c) inclination. The histograms represent the observed population (updated to February 2016), with diagonal filling for NEAs discovered during the last 18 months, while the error bars represent the modeled population.

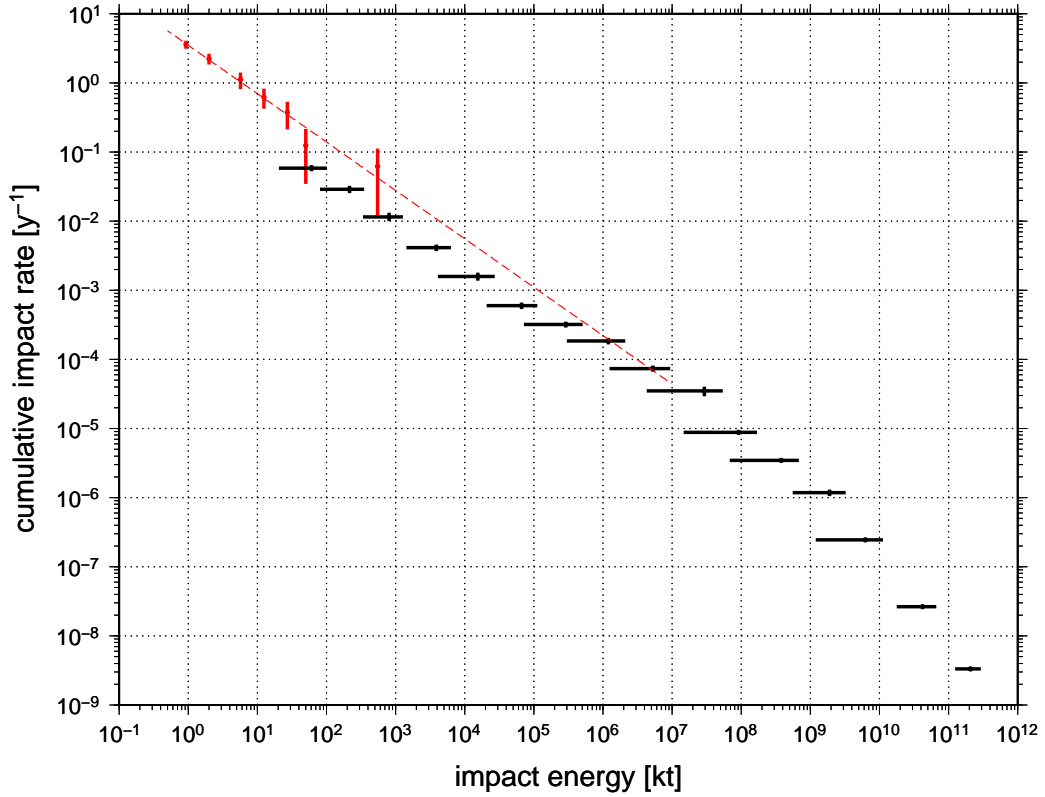


Fig. 5.— Cumulative Earth impact rate for NEAs as a function of the impact energy (black). The bolide data (Brown et al. 2013) is in red (error bars are counting statistics only), with an average power law of  $n = 3.5E^{-0.7}$  with  $n$  impact rate and  $E$  impact energy (red dashed line). The assumed mean density of NEAs is  $3,000 \text{ kg m}^{-3}$  and geometric albedo  $p_V = 0.14$ . The impact energy uncertainty includes contributions from the impact velocity range as well as the size range in each magnitude bin.

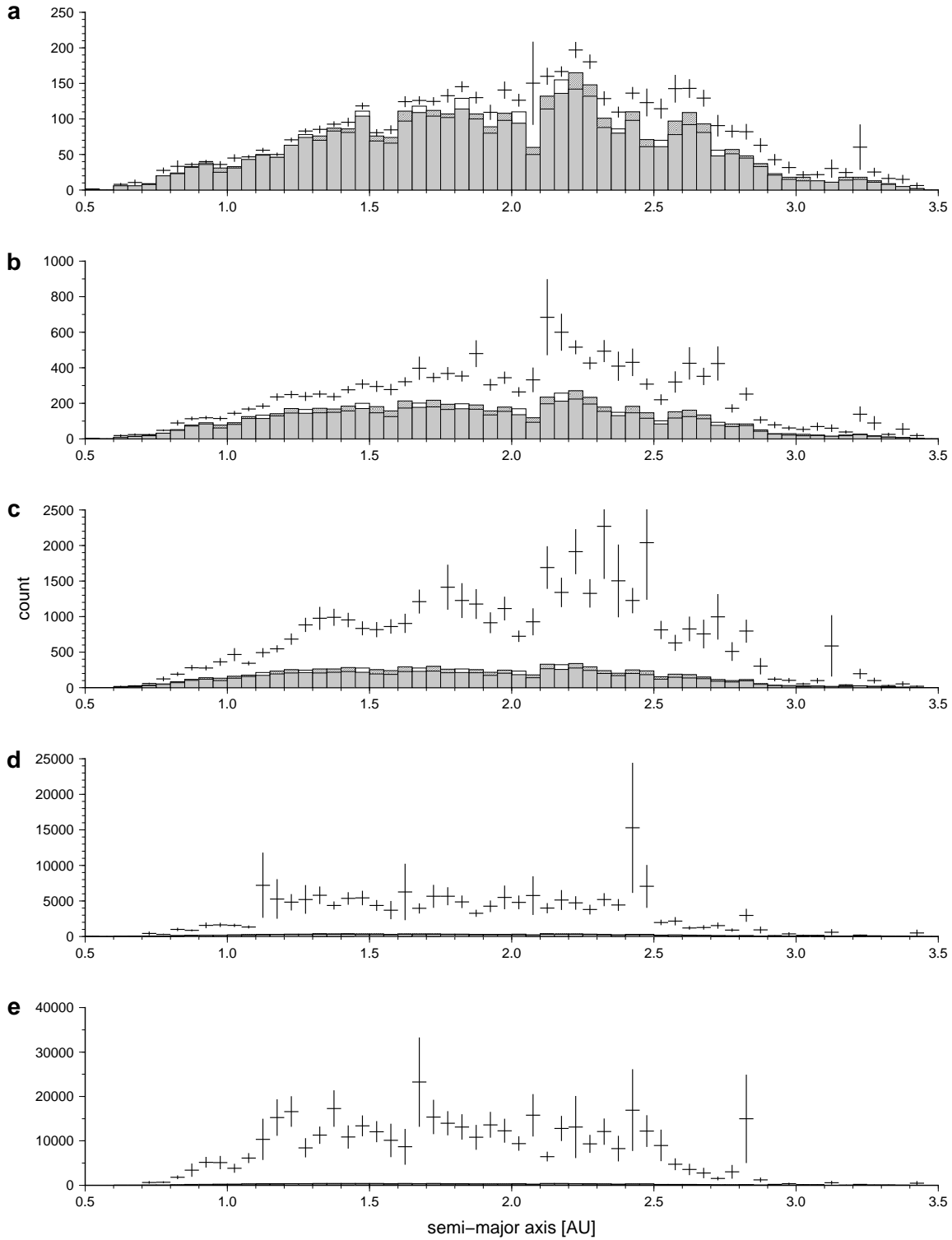


Fig. 6.— Distribution of the population of NEAs in semi-major axis for bodies with absolute magnitude up to (a)  $H < 20$ , (b)  $H < 22$ , (c)  $H < 24$ , (d)  $H < 26$ , (e)  $H < 28$ . The histograms represent the observed population (updated to February 2016), with diagonal filling for NEAs discovered during the last 18 months, while the error bars represent the modeled population.

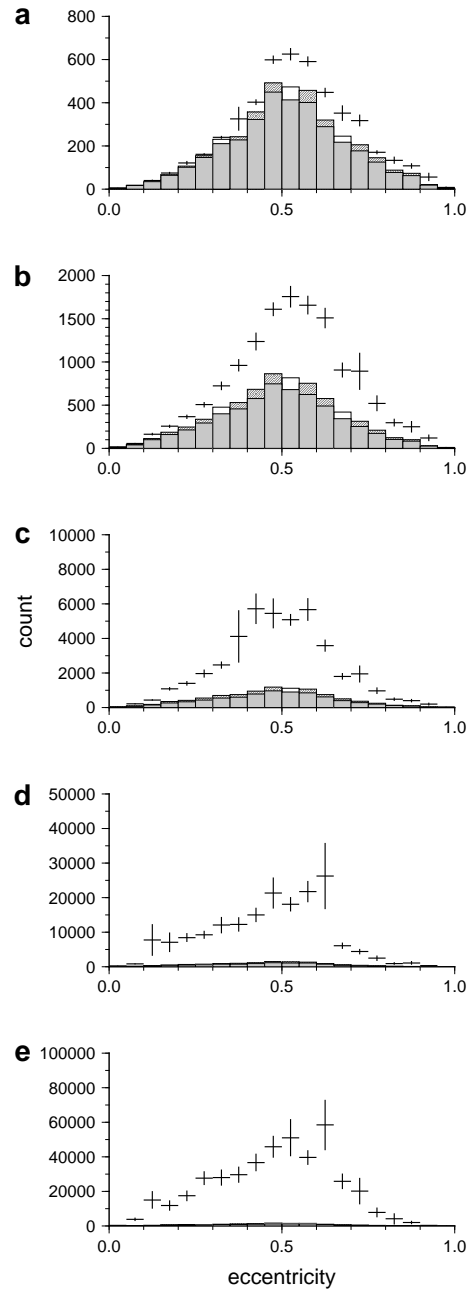


Fig. 7.— Distribution of the population of NEAs in eccentricity, same conventions as Figure 6.

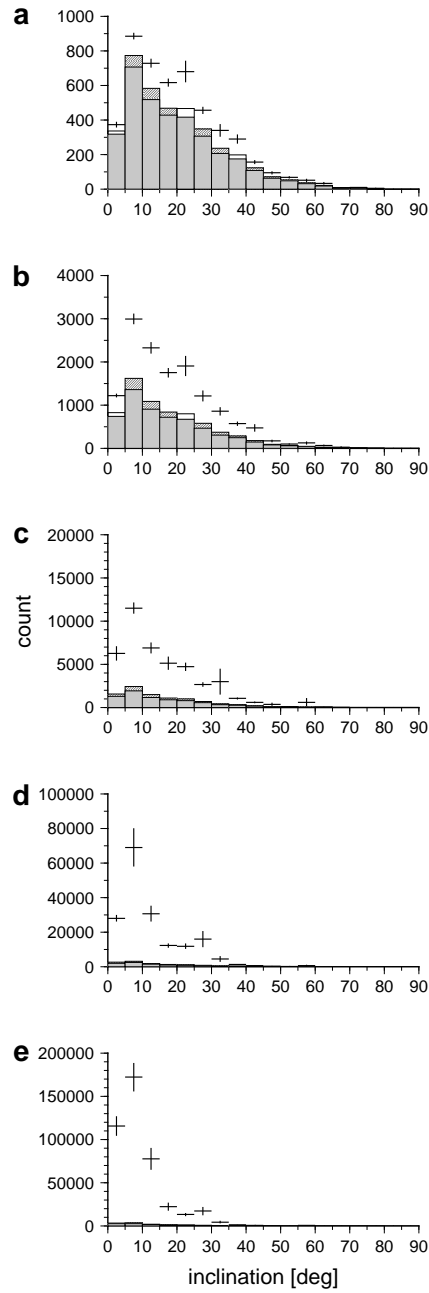


Fig. 8.— Distribution of the population of NEAs in inclination, same conventions as Figure 6.

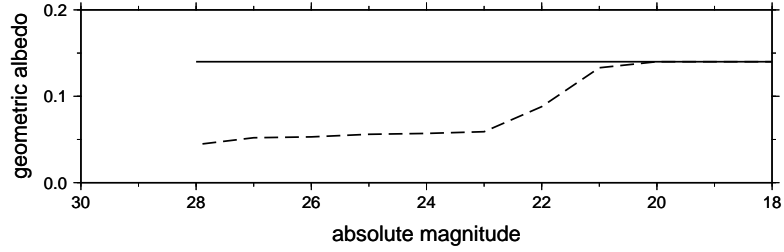


Fig. 9.— Geometric albedo of NEAs: nominal average value  $p_V = 0.14$  (continuous line) versus dynamic value to match the extrapolated bolide data (dashed line), see Figure 5.

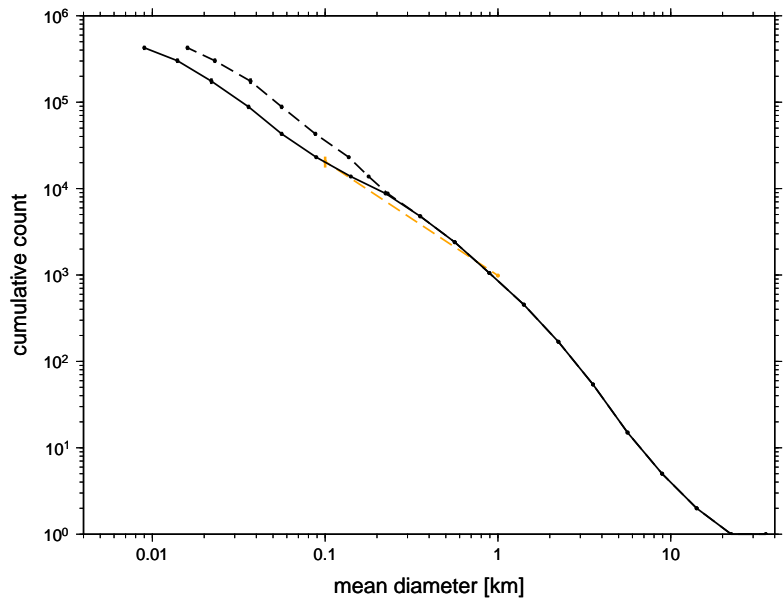


Fig. 10.— Cumulative size-frequency distribution of NEAs: using the nominal geometric albedo  $p_V = 0.14$  (continuous line) versus using the dynamic albedo (dashed line), see Figure 9. The orange data are from Mainzer et al. (2011).